Rare Metal Materials and Engineering
Volume 49, Issue 12, December 2020
Available online at www.rmme.ac.cn

Science Press

Cite this article as: Rare Metal Materials and Engineering, 2020, 49(12): 4031-4040.

ARTICLE

Anisotropy in Microstructure and Impact Toughness of 316L Austenitic Stainless Steel Produced by Selective Laser Melting

Zong Xuewen[1], Liu Wenjie[1], Yang Yumeng[2], Zhang Shuzhe[3], Chen Zhen[3]

[1] School of Mechanical Engineering, Xi'an University of Science and Technology, Xi'an 710054, China; [2] AVIC Optoelectronic Technology Co., Ltd, Luoyang 471023, China; [3] School of Mechanical Engineering, Xi'an Jiaotong University, Xi'an 710049, China

Abstract: Anisotropy of microstructure and impact toughness of 316L austenitic stainless steel fabricated by selective laser melting (SLM) was studied. The microstructures were characterized by optical microscope (OM), X-ray diffraction (XRD), scanning electron microscope (SEM) and electron backscatter diffraction (EBSD). The impact toughness tests were carried out using a metal pendulum tester. The results show that both the microstructure and impact toughness of SLM processed 316L stainless steel exhibit a fancy anisotropy. The phase in the *X*/*Y* and *Z* direction is the γ-Fe phase, and its structure perpendicular to *Z* direction is in a checkerboard morphology. Most of the grains are refined (d_{mean}=9.177 μm) and show equiaxed morphology, especially in the overlapped area of the molten pool, grains are observed to be finer (maximum 6 μm). However, the columnar grain parallel to the *Z* direction resembles a fish-scale pattern, with an average diameter of 21.247 μm. Meanwhile, the texture perpendicular to the *Z* direction exhibits a strong fiber texture <110>//rolling direction (RD) and a weak plate texture {112}<110>, while the texture parallel to the *Z* direction exhibits a strong fiber texture <110>//RD. Under a similar density condition, the impact toughness of *X*/*Y* direction and *Z* direction is 62.8±3.2 and 38.6±4.5 J, respectively, and the impact toughness of the *X*/*Y* direction is 62.69% higher than that of the *Z* direction. Also, grain size, grain boundary misorientation and texture type have an significant effect on the anisotropy of impact toughness. The grains perpendicular to the building direction are also refined with an increased grain boundaries with large angles and an enhancement in the grain toughness. Since the fiber texture <110>//RD shows a low impact toughness resistance, plate texture {112}<110> exhibits a good impact toughness resistance, and the <110>//RD texture perpendicular to the *Z* direction has low strength and weak {112}<110> texture exists, the impact toughness of *X*/*Y* direction is preferred.

Key words: laser selective melting; 316L austenitic stainless steel; microstructure; texture; impact toughness; anisotropy

316L stainless steel is a typical ultra-low carbon austenitic stainless steel, which is characterized by high corrosion resistance, good biocompatibility, high oxidation resistance and excellent comprehensive mechanical properties, and widely used in aerospace, petrochemical, automotive industry and biomedical fields [1-3]. In recent years, the preparation of some specific and complex parts of aircraft 316L stainless steel by selective laser melting (SLM) has been a research focus. Through comparison with the traditional molding technology, it has the advantage of producing arbitrarily complex parts without any requirement for mold, thus shortening the production cycle [4,5]. Up to now, researches are mainly focused on exploring the characteristics of 316L stainless steel powder, optimization of the process parameters, density and mechanical properties. Kamath et al[6] processed 316L stainless steel samples with a laser power of 400 W, layer thickness of 30 μm and scanning speed of 300~800 mm/s, and the density reached approximately 99.3%~99.5%. Casati et al [7] analyzed the microstructure and fracture behavior of SLM processed 316L austenitic stainless steel to

Received date: April 17, 2020
Foundation item: National Natural Science Foundation of China (51875452, 51804251)
Corresponding author: Zong Xuewen, Ph. D., Associate Professor, School of Mechanical Engineering, Xi'an University of Science and Technology, Xi'an 710054, P. R. China, Tel: 0086-29-85583159, E-mail: zongw007@xust.edu.cn

investigate the influence of processing mode on microstructure, texture, and tensile fracture mechanism. Suryawanshi et al[8] studied the quasi-static mechanical properties of 316L stainless steel processed by SLM to obtain the crack propagation mechanism during the process. Wang et al [9] produced 316L stainless steel by SLM and found that the yield strength and tensile ductility performance of 316L stainless steel are both higher than those of the traditional manufacture. Gray et al[10] investigated the dynamic compression mechanical properties and spalling characteristic of 316L stainless steel materials prepared by SLM, and discussed the effect of heat treatment on the quality of SLM. Yasa et al[11] studied the influence of heat treatment methods on the impact toughness of 316L stainless steel formed by SLM. Wu et al [12] investigated the anisotropy of impact toughness of TC4 titanium alloy formed by SLM and analyzed the influence of different forming defects on impact toughness. However, there is inadequate systematic research on the impact toughness of SLM-fabricated 316L stainless steel, especially the relationship among microstructure, texture, fracture behavior and toughness.

In this study, 316L stainless steel impact test samples were successfully prepared by SLM. The microstructure, textures, fracture behavior and the impact toughness of the impact specimens in the *X*/*Y* and *Z* directions were studied, which provides a certain reference for the application of 316L stainless steel.

1 Experiment

In this research, 316L stainless steel metal powder was atomized with water, and the chemical composition of the powder is shown in Table 1. The powder particles are approximately regular spheres with a diameter of 20~80 μm, and the average particle size is 37.058 μm, as shown in Fig.1. The oxygen content of the powder is less than 500 μL/L, and the powder flowability is less than 18 s/50 g. Rectangular samples were processed by the SLM150 system (China Zhongrui 3D Technology Co., Ltd). A scanning angle rotating by 67° around the *Z*-axis for each layer was adopted, as shown in Fig.2a. The experiment was carried out in a nitrogen-protected environment, with an oxygen concentration below 100 μL/L. The models were placed on the construction platform with a maximum size of 150 mm×150 mm×200 mm, and a weight capacity of 20 kg. The fiber laser had a maximum output of 500 W, a laser wavelength of 1064 nm and a spot diameter of 70 μm. The optimized parameters were adopted: laser power 200 W, scan speed 800 mm/s, hatching space 0.06 mm and layer thickness 0.03 mm. The size of the fabricated impact sample was 55 mm×10 mm×10 mm, as shown in Fig.2b.

Table 1 Chemical composition of 316L stainless-steel powder (wt%)

Cr	Ni	Mo	Si	Mn	P	Fe
17.92	12.04	2.42	0.52	0.051	0.035	Bal.

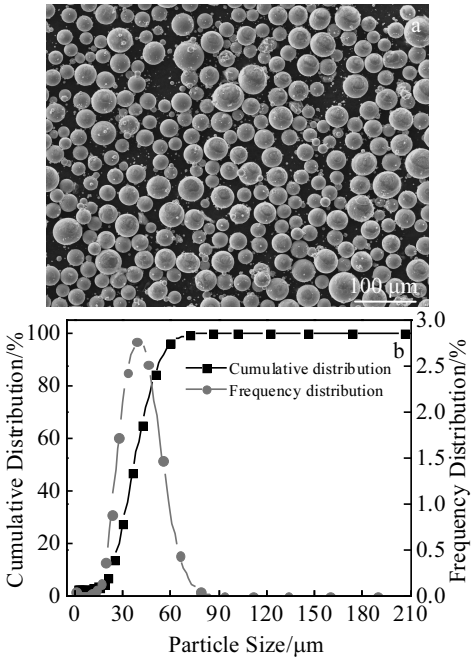

Fig.1 SEM image of 316L austenitic stainless-steel powder (a) and powder particle size distribution (b)

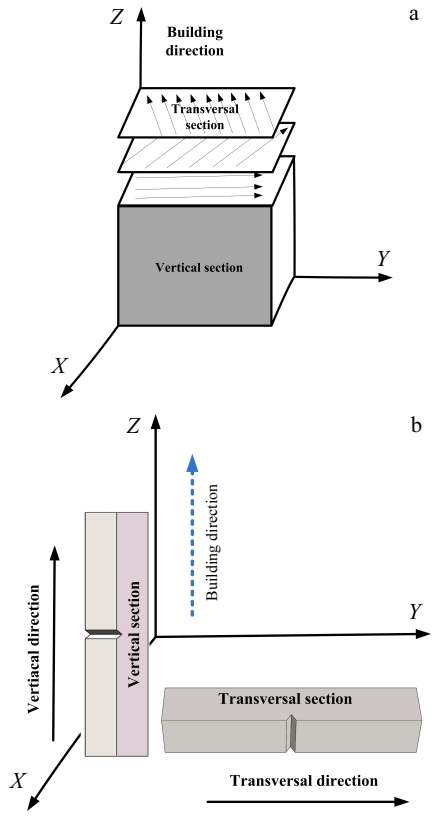

Fig.2 Scanning mode of 316L austenitic stainless-steel (a) and schematic diagram of impact samples (b)

The *XY* plane of the transverse samples and *XZ* plane of the vertical samples were taken for the structure analysis. An observed area was plane composed of a transverse (TD) and a rolling direction (RD), which was the building direction EBSD observation. It was performed using JSM-7001F field emission scanning electron microscope equipped with an SEM-EBSD system on an electron microscope. XRD was used for phase analysis. After the observation, the specimen was prepared by side grinding and polishing, and its metallographic structure was observed by aqua regia corrosion. The impact samples formed by SLM were tested by the ZBC2000 series metal pendulum testing machine and the pendulum energy was set as 150 J. Under the condition of normal temperature 21 °C, the specimen was impacted, and the fracture morphology of the specimen was analyzed.

2 Results and Discussion

2.1 Microstructure

Fig.3 shows the optical micrographs of the SLM processed samples in the *XY* plane and *XZ* plane. As shown in Fig.3a and 3b, the morphology of the molten pool in the *XY* plane of the sample has a checkerboard pattern, the lapping effect is good, and there are no holes and lap defects on the surface. According to Fig.3c and 3d, the morphology of the molten pool in the longitudinal section of the sample looks like a fish-scale [13], the overlap rate is high, and no pores are found on the surface. Also, the height of the molten pool is 50~70 μm and the width is 100~130 μm. This is a combined effect of the temperature gradient of the molten pool that is directly determined by laser energy density, the fluidity of the molten metal and the overlap effect between the melting channels, thus promoting the stability of the molten pool and the overlap rate of the sample formation.

Fig.4a shows that the *XY* plane morphology of the grains are equiaxed morphology, the grain size is small with an average diameter of 9.177 μm, and the grain diameter is distributed in the range of 1.692~70.175 μm with a dispersion degree of 9.582. In particular, the grains in the re-melting area of the melting pool are fine (below 6 μm), as shown in Fig.5, which is a result of twice laser scanning upon the overlapped area, making the grain size finer after re-melting[13,14]. As can be seen from Fig.4b, most of the grains in the *XZ* plane are columnar crystal morphology, the grain size is large with an average diameter of 21.247 μm, and the grain diameter is distributed in the range of 5.136~97.694 μm with a dispersion degree of 15.382. The main distribution is about 15 μm, the grain distribution in adjacent regions is not obvious and the grain size is larger than that in the *XY* plane.

Through the above comparison, grains in the *XY* plane are refined and the average diameter is reduced by 66.32% compared to the *XZ* plane. An obvious difference in adjacent grains is observed, with a low degree of dispersion, but the dispersion degree is low. Meanwhile, according to the Hall-Petch relationship, the mechanical properties depend on the size of grains, grain morphology and texture[15,16]:

$$\sigma_s = \sigma_0 + Kd^{-\frac{1}{2}} \quad (1)$$

where σ_s is the yield strength, σ_0 is the material correlation coefficient, K is the coefficient of grain boundary's influence on strength, and d is grain size. According to the dislocation theory, the stress is concentrated in the grain boundary, and if the dislocation accumulation and stress are high enough,

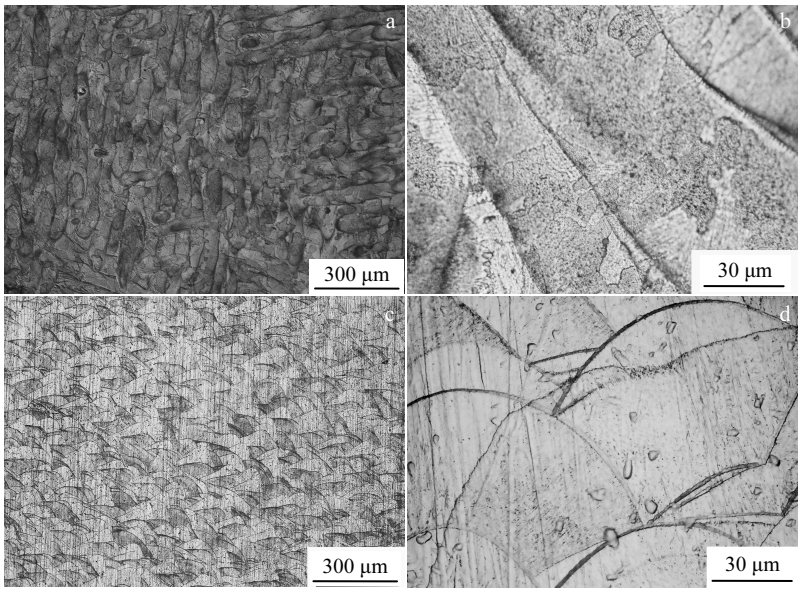

Fig.3 Optical micrographs of SLM-ed 316L samples: (a, b) *XY* plane and (c, d) *XZ* plane

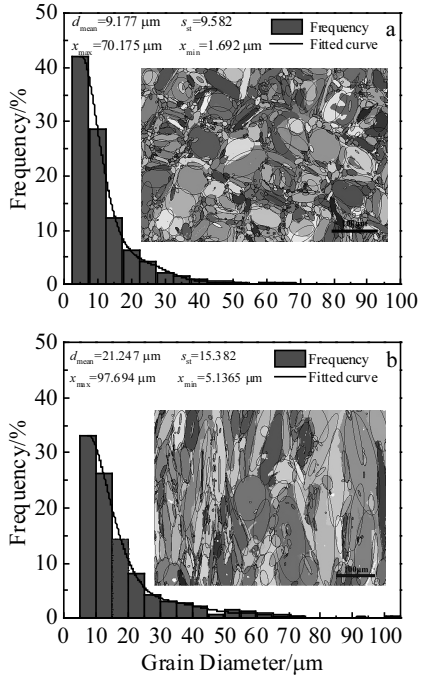

Fig.4 Grain size distribution of SLM-ed 316L samples: (a) *XY* plane and (b) *XZ* plane

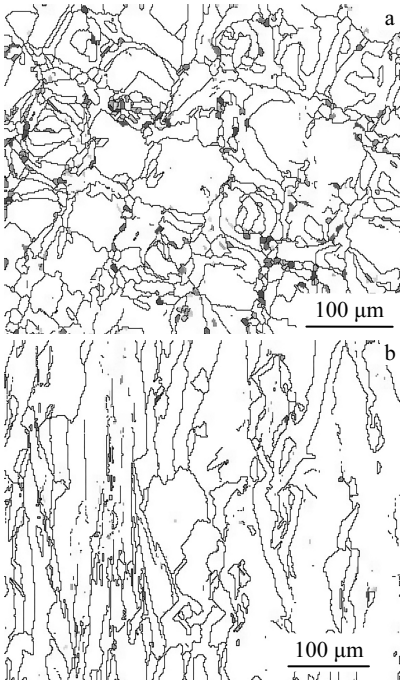

Fig.5 Ultra-fine grain distribution of SLM-ed 316L samples: (a) *XY* plane and (b) *XZ* plane

slippage will spread from one grain to another, and then yield occurs[17]. Therefore, the grain of the *XY* plane is refined and the properties of the material are well promoted.

Fig.6 shows the distribution of grain orientation obtained by EBSD; the small-angle grain boundary (LAGBs, $\theta \leq 15°$) and large-angle grain boundary (HAGBs, $\theta > 15°$) are represented by green and black, respectively. As shown in Fig.6, LAGBs on the *XY* plane and *XZ* plane are 73.14% and 88.45%, respectively, indicates that LAGBs are more suitable for the building direction of SLM processed samples. HAGBs on the *XY* plane are higher than on the *XZ* plane, because the repeated re-melting of the adjacent fusion pool promotes the grain refinement and the increase of HAGBs. It is well known that LAGBs are caused by severe deformation, which also indicates the density of dislocation, so the more LAGBs, the more dislocation. However, HAGBs are usually expressed as recrystallized grain boundaries[15]. Therefore, the *XY* plane with large LAGBs obtains a preferred match of strength and toughness.

However, the deformation of the sample is not uniform due to different deformation capacities of the crystals. Fig.7 shows the Schmid factor (SF) distribution of SLM samples, in which different colors represent different crystal deformation capacities. As the values changes from 0 to 0.50 (color changes from blue to red), the crystal changes from hard to soft orientation[18]. As shown in Fig.7, the value of the Schmid factor of the samples in both directions ranges from 0.28 to 0.5, so the crystals of SLM processed samples exhibit soft orientation ability. It is well known that the plastic deformation of a single crystal at the microscopic scale is characterized by slip and twinning and belongs to shear strain. On the slip plane, the critical sectorial stress along the slip direction and the applied normal stress obey the following formula:

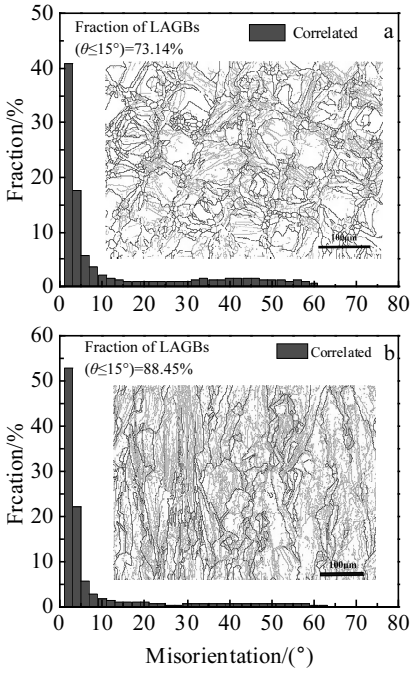

Fig.6 Grain orientation difference and distribution of SLM-ed 316L samples: (a) *XY* plane and (b) *XZ* plane

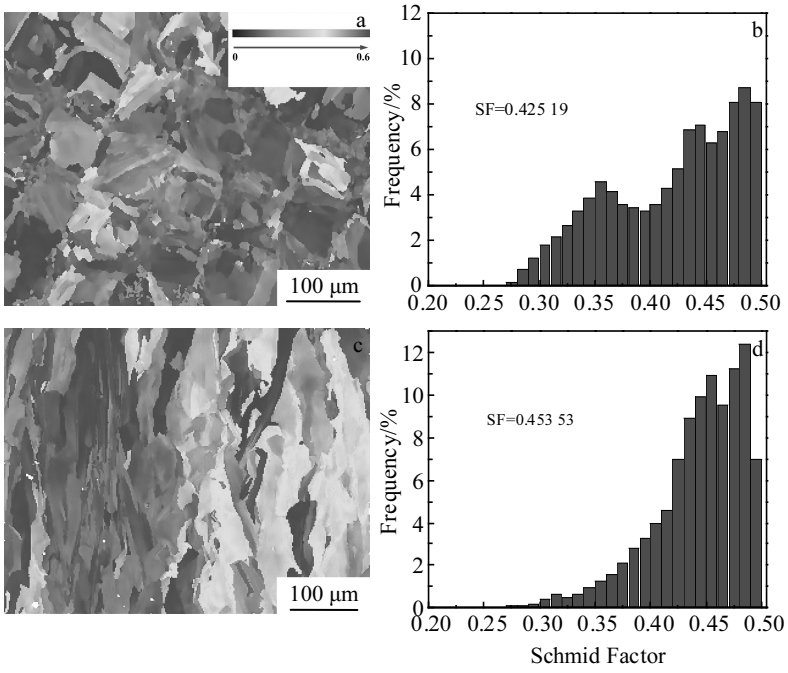

Fig.7 Schmid factor distribution of SLM-ed 316L samples: (a, b) *XY* plane and (c, d) *XZ* plane

$$\tau_\sigma=\sigma_s \cos\lambda\cos\varphi \quad (2)$$

where SF=cosλcosφ, φ is the angle between stress and the direction normal to the slid plane, λ is the angle between stress and the sliding direction, τ_σ is the material coefficient, and σ_s is material yield strength. The larger the Schmid factor, the easier the slip system to initiate, and the easier the material to deform, then lowering the yield strength[19]. Fig.7b and 7d show that the Schmid factor values of the *XY* plane and *XZ* plane are 0.425 19 and 0.453 53, respectively. Therefore, the *XZ* plane slip system is easier to initiate, and the material is easier to deform.

Fig.8 shows the local misorientation difference distribution (LMAA) of SLM processed samples. As shown in Fig.8a and 8b, the average local misorientation, the maximum misorien-

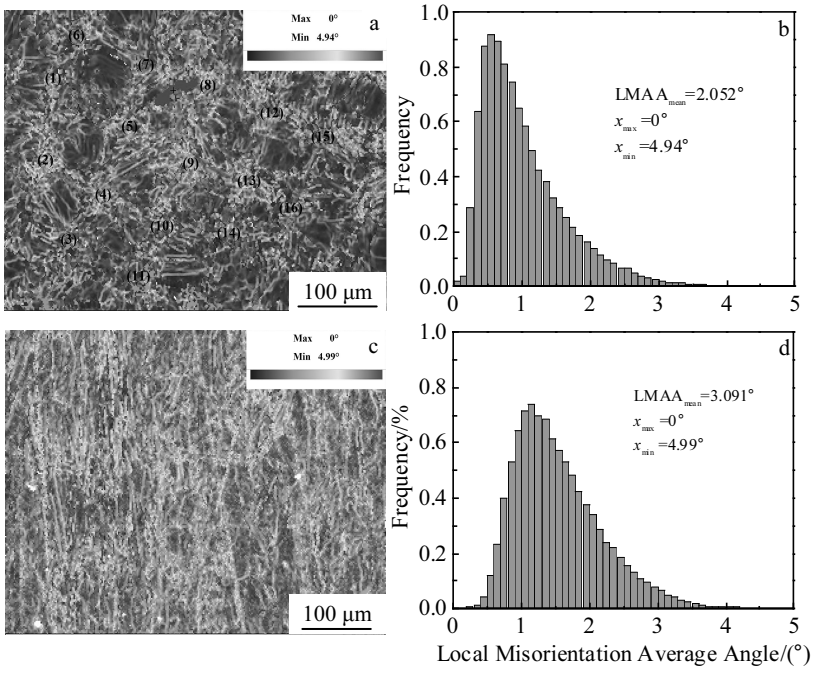

Fig.8 Local misorientation distribution of SLM-ed 316L samples: (a, b) *XY* plane and (c, d) *XZ* plane

tation, and the minimum misorientation on the *XY* plane are 2.050°, 4.94°, and 0°, respectively. The higher local misorientation is mainly distributed in the overlapped area. As shown in Fig.8c and 8d, the average local misorientation, the maximum misorientation, and the minimum misorientation on the *XZ* plane are 3.091°, 4.99°, and 0°, respectively. Since LMAA qualitatively denote the uniformity of plastic deformation, a higher value indicates a greater degree of plastic deformation[20]. Therefore, the degree of plastic deformation of the *XY* plane is small, but the strength is high, and the local misorientation of the *XY* plane is related to the re-melting region.

2.2 Phase analysis

According to the XRD patterns (Fig.9), the phase of the *XY* plane and *XZ* plane of SLM samples and the powder is mainly composed of the *γ*-Fe phase (fcc). In comparison with the standard austenitic powder 316L, the diffraction peaks of (111) and (200) of the *XY* plane and *XZ* plane of the SLM processed samples change greatly. In the *XY* plane, the peak value of (111) diffraction increases by about two times, the peak strength of (200) increases by about two times, and the intensity of other diffraction peaks also changes to some extent. In the *XZ* plane, the peak value of (111) diffraction increases by approximately three times, and the peak strength of (200) increases by about 1.5 times. This indicates that the building direction has a significant effect on the formation of texture in SLM.

2.3 Texture analysis

As shown in Fig.10, on the *XY* plane, the grain direction distribution is slightly random, but the re-melting zone is mainly on the (101) plane. However, on the *XZ* plane, grain direction distribution is mainly along (111) and (101) plane; this indicates that the grain has a strong crystal orientation <110> in the *XZ* plane, and the grain orientation is random in the *XY* plane. It can be seen from the pole figure (Fig.11) that the *XY* plane has a strong fiber texture <110>//RD (texture intensity of 7.83) and a weak plate texture {112}<110>, while the *XZ* plane is mainly composed of a strong fiber texture <110>//RD (texture intensity of 12.23), which is due to the high-temperature gradient and the fast cooling rate (10^5 K/s) in SLM process[21,22]. This is further confirmed by the orientation distribution function (Fig.12).

2.4 Impact toughness

Fig.13 shows the impact energy of SLM processed samples in *X*/*Y* direction and *Z* direction with value of 62.8±3.2 J and 38.6±4.5 J, respectively. The impact energy of the *X*/*Y* direction is higher than that of the *Z* direction and increases by 62.69%, but the density of samples in both directions is 99.6%. This shows that even if the relative density of the two samples is the same, the forming direction has a significant effect on the impact toughness of SLM processed 316L samples. Therefore, the 316L stainless steel sample formed by SLM has obvious anisotropy of impact toughness.

2.5 Impact fracture morphology

Fig.14 shows the fracture morphologies of impact samples in both the *X*/*Y* direction and *Z* direction. As shown in Fig.14a~14c, the impact fracture morphology of the transversal samples is macroscopically flat with a large number of dimples dispersed on the surface, and the tearing ridge is less noticeable. As shown in Fig.14d~14f, the impact fracture morphology of the vertical samples shows that the tearing is larger and the dimples are smaller and less noticeable. Through the comparison, it can be seen that the fracture surface of transverse samples are characterized by large and deep dimples, which indicates more impact energy absorption during the impact test, and consequently

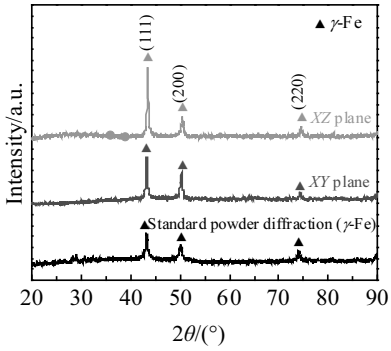

Fig.9 XRD patterns of SLM-ed 316L samples

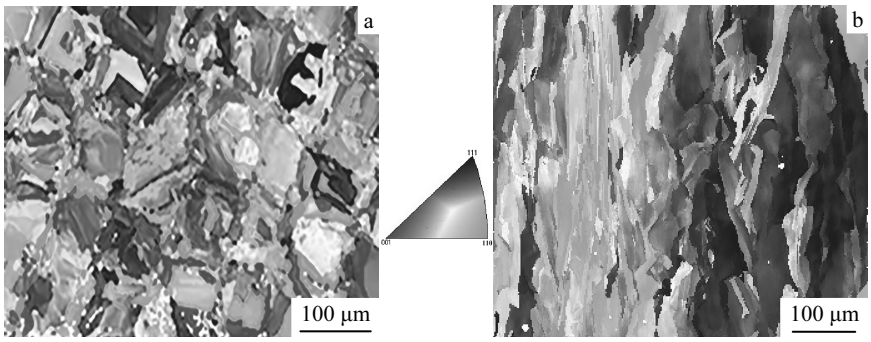

Fig.10 Grain orientation distribution of SLM-ed 316L samples (IPF): (a) *XY* plane and (b) *XZ* plane

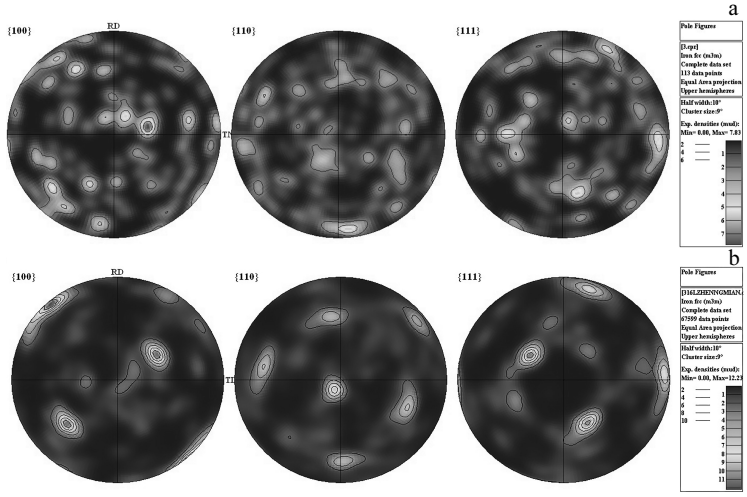

Fig.11 Polar figure of SLM-ed 316L samples (IPF): (a) *XY* plane and (b) *XZ* plane

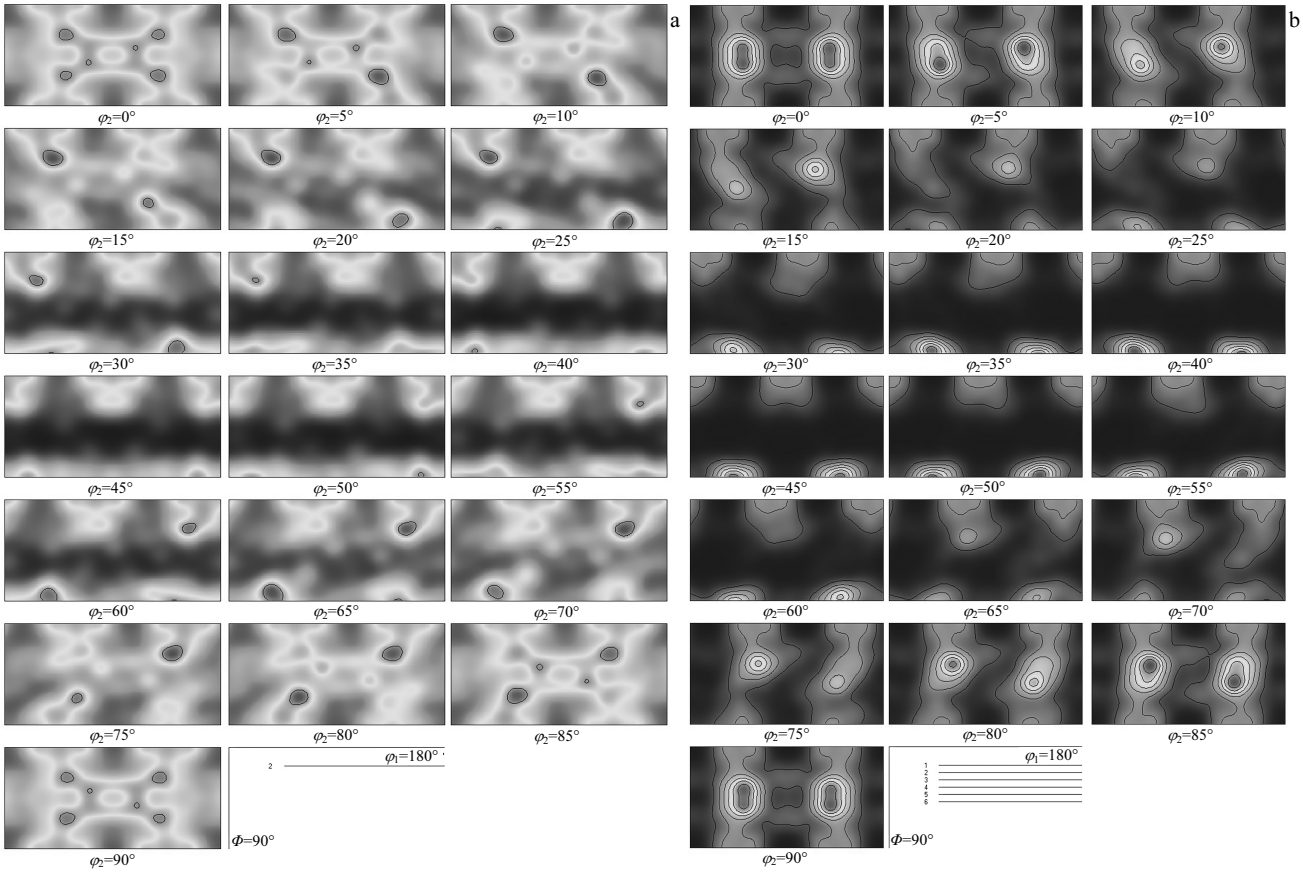

Fig.12 Orientation distribution function (ODF) of SLM-ed 316L samples: (a) *XY* plane and (b) *XZ* plane

it has good toughness. This shows that the impact toughness of 316L stainless steel samples processed by SLM is different in the *X*/*Y* direction and *Z* direction.

2.6 Discussion

2.6.1 Effect of grain size and grain boundaries on impact toughness

The basic relationship between the grain size and toughness is that the refined grains can improve the toughness. When more finer grains are subjected to external forces, the strain difference between inside and outside of the grains can be reduced, which reduces the stress concentration and develops a uniform force within the material, and it is not easy to crack[23].

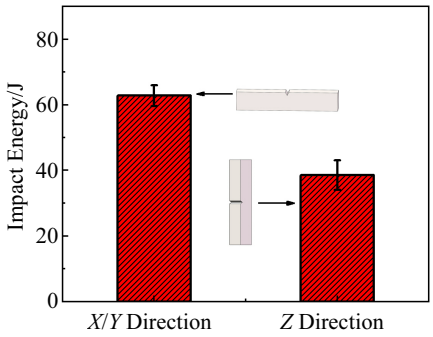

Fig.13 Impact energy of SLM processed samples in *X*/*Y* direction and *Z* direction

Grain size has a great influence on cleavage fracture strength, and the relationship between cleavage fracture strength and grain size is as follows[24-26]:

$$\sigma_{\mathrm{f}} = \sqrt{\frac{4G\gamma}{d}} \propto d^{-\frac{1}{2}} \tag{3}$$

where σ_{f} is cleavage fracture strength, d is the grain diameter, G and γ are the shear modulus of the metal and the surface energy of crack, respectively. Refining grains can improve cleavage fracture strength while lower the ductile-brittle transition temperature (T_{c}) [27]. SLM processed 316L austenitic stainless-steel undergoes a high-temperature gradient and extremely fast cooling rates, resulting in significant differences in grain sizes in the *X*/*Y* direction and *Z* direction. As shown in Fig.4 and Fig.5, the average grain diameter of the *XY* plane grains is 9.177 μm. In particular, the average grain diameter in the fusion pool re-melting area is smaller than 6 μm, while the grain diameter in the *XZ* plane is 21.247 μm, Therefore, grains are refined in the *X*/*Y* direction of SLM samples, leading to an increased grain boundaries and consequently an increased cleavage fracture strength, and decreased ductile brittle transition temperature. There is apparent impact toughness

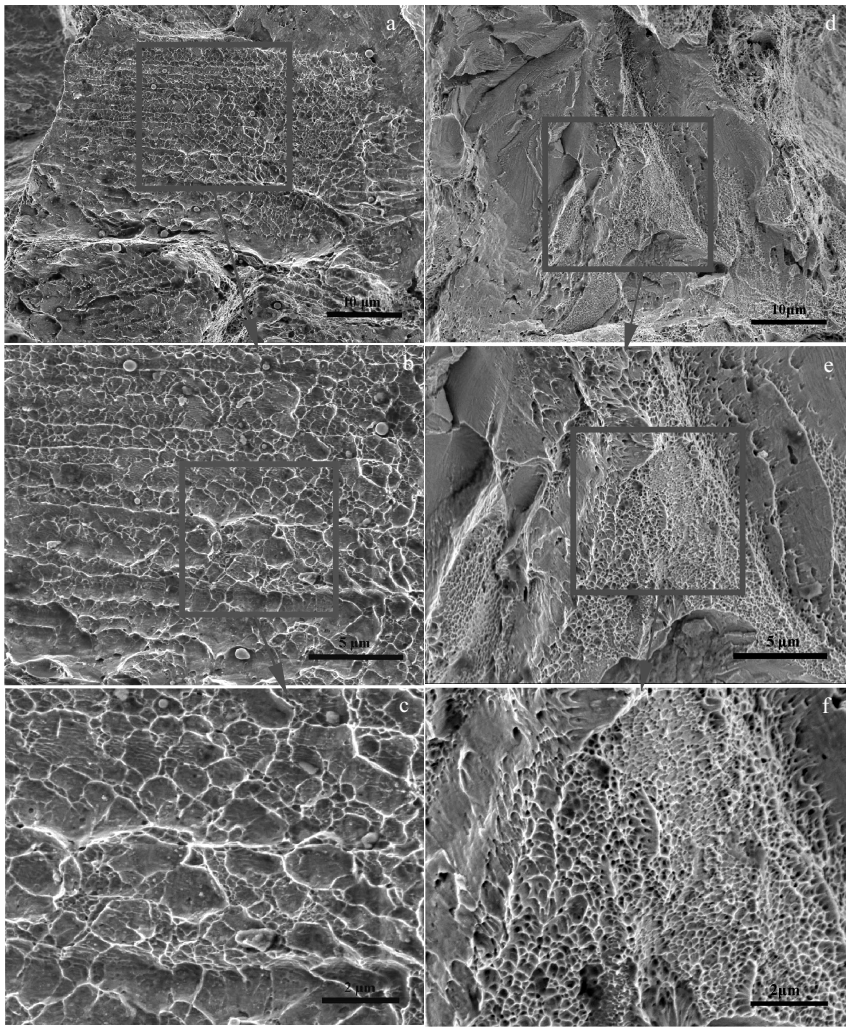

Fig.14 Fracture morphologies of impact samples: (a~c) *X*/*Y* direction and (d~f) *Z* direction

anisotropy in the SLM samples.

The effect of small-angle grain boundary on cleavage crack is weak, and the brittle crack cannot be stopped effectively. Whereas the effect of large-angle grain boundary on cleavage crack is strong[28,29], as the number of large angular grain boundaries increases, the cleavage crack growth is hindered. As shown in Fig.15, the portion of large-angle grain boundary of the *XY* plane is 26.86%, which is increased by 1.33 times compared to that of *XZ* plane (11.55%), and large-angle grain boundary in the *XY* plane and *XZ* plane is 26.86% and 11.55%, respectively. Since the *XY* plane has finer grains with large grain boundary where the atoms are disorderly arranged, crack deflection occurs and crack propagation can be effectively resisted, thus improving the impact toughness. As a result, the large-angle grain boundary of 316L stainless steel formed by SLM has an obvious influence on the impact toughness anisotropy.

2.6.2 Effect of texture on impact toughness

The strength and toughness of material strongly depend on its texture[30,31]. However, the relationship between the texture types and mechanical properties is yet to be established[32]. Yang et al[30,31] studied the effect of texture and layering on ductile anisotropy in API X100 pipeline steel, and it was found that texture type and strength have obvious influence on the anisotropy of impact toughness, while {001}<110> texture is bad for toughness and makes steel brittle, and the texture of {112}<110> and {332}<113> can obtain better impact performance. As shown in Fig.8~10, there are strong fiber texture <110>//RD and weak sheet texture {112}<110> on the *XY* plane of SLM processed 316L stainless steel samples, while the *XZ* plane has much stronger fiber texture <110>//RD than the *XY* plane. Analysis has shown that the fiber texture <110>//RD is bad for the impact toughness, while the sheet texture {112}<110> is good for the toughness. Therefore, contrast to the *XZ* plane, the *XY* plane <110>//RD has low texture strength, and the existence of {112}<110> texture improves the toughness. Meanwhile, combined with Fig.12, it is obvious that the toughness of the *XY* plane is better than that of the *XZ* plane, and texture leads to obvious anisotropy of impact toughness.

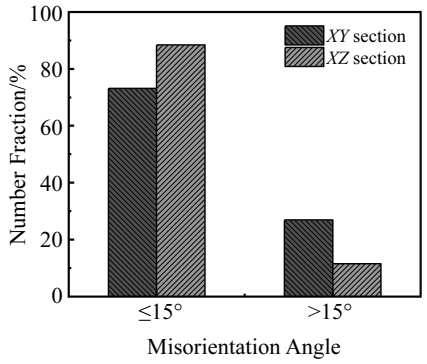

Fig.15 Grain boundary distribution of SLM-ed 316L samples

3 Conclusions

1) In the SLM process, the extremely high-temperature gradient and rapid cooling rate (10^5 K/s) promote the non-equilibrium transformation of the molten pool and the formation of ultrafine grains, resulting in anisotropy of microstructure and mechanical properties.

2) The microstructure of 316L austenitic stainless steel processed by SLM has obvious anisotropy. The microstructure perpendicular to *Z* direction has checkerboard morphology, and grains are mostly equiaxed morphology and refined (d_{mean}= 9.177 μm). In particular, the grains in the re-melting area of the molten pool are finer (below 6 μm). The microstructure in *Z* direction shows a fish-scale morphology, and most of grains are columnar morphology with larger grain diameters (d_{mean}=21.247 μm) and small angle grain boundaries.

3) The Schmid factors perpendicular and parallel to the building direction are 0.425 19 and 0.453 53, respectively. All crystals belong to soft orientation, and the average local misorientation perpendicular to the *Z* direction is small. Therefore, the plastic deformation is low, but the strength is high. Meanwhile, the local misorientation perpendicular to *Z* direction has an obvious relationship with the re-melting area.

4) Phases perpendicular and parallel to the building direction of SLM processed 316L stainless steel are *γ*-Fe phase. Microstructure in the direction perpendicular to the *Z* direction has strong fiber texture <110>//RD and weak sheet texture {112}<110>, while in the direction parallel to the *Z* direction, it is strong fiber texture <110>//RD. It is further confirmed that the increase of peak strength at (100), (200) and (220) is related to the formation of texture.

5) The impact toughness of SLM processed 316L austenitic stainless steel has obvious anisotropy. The density is 99.6% in both *X*/*Y* direction and *Z* direction, but the impact energy is 62.8±3.2 and 38.6±4.5 J, respectively; the impact toughness of the transversal section is 62.69% higher than that of the vertical. Meanwhile, grain size, high angle boundary and texture type have significant effects on anisotropy of impact toughness. The grains in plane perpendicular to the building direction are refined with a large number of high angle grain boundaries, the cleavage fracture strength increases and the ductile and brittle transition temperature is reduced, so the toughness is better. Since fiber texture <110>// RD is bad for impact toughness, and plate texture {112}<110> is good for toughness, the strength of the direction perpendicular to the building direction with strong texture of <110>// RD and weak {112}<110> texture is lower than that parallel to the building direction, but the toughness of *X*/*Y* direction is better.

References

1 Li X, Willy H J, Chang S *et al*. *Materials & Design*[J], 2018, 145: 1

2 Li Kaishang, Peng Jian. *Journal of Materials Engineering*[J], 2018, 11: 148

3 Zainab M A R, Farag M M, Abdel G N A *et al*. *Surface & Coatings Technology*[J], 2018, 334: 479
4 Santos E C, Shiomi M, Osakada K *et al*. *International Journal of Machine Tools & Manufacture*[J], 2006, 46(12): 1459
5 Duan Xiaoxi, Gao Shiyou, Gu Yongfei *et al*. *Chinese Journal of Lasers*[J], 2016, 43(1): 103 004 (in Chinese)
6 Kamath C, El-Dasher B, Gallegos G F *et al*. *International Journal of Advanced Manufacturing Technology*[J], 2014, 74(1-4): 65
7 Casati R, Lemke J, Vedani M. *Journal of Materials Science & Technology*[J], 2016, 8: 738
8 Suryawanshi J, Prashanth K G, Ramamurty U. *Materials Science and Engineering A*[J], 2017, 696: 113
9 Wang Y M, Voisin T, Mckeown J T *et al*. *Nature Materials*[J], 2017, 17(1): 63
10 Gray G T, Livescu V, Rigg P A *et al*. *Acta Materialia*[J], 2017, 138: 140
11 Yasa E, Deckers J, Kruth J P *et al*. *Virtual and Physical Prototyping*[J], 2010, 5(2): 89
12 Wu Mingwei, Lai Panghsin Chen J K *et al*. *Materials Science & Engineering A*[J], 2016, 650: 295
13 Xu Jiayu, Ding Yutian, Hu Yong *et al*. *Rare Metal Materials and Engineering*[J], 2019, 48(11): 3727 (in Chinese)
14 Tomus D, Tian Y, Rometsch P A *et al*. *Materials Science and Engineering A*[J], 2016, 667: 42
15 Liu Zhangguang, Li Peijie, Xiong Liangtong *et al*. *Materials Science & Engineering A*[J], 2017, 680: 259
16 Lv Xudong, Wen Bo, Du Jinhui. *Rare Metal Materials and Engineering*[J], 2019, 48(5): 1386
17 Niels Hansen. *Scripta Materialia*[J], 2004, 51(10): 801
18 Yan Zhifeng, Wang Denghui, He Xiuli *et al*. *Materials Science & Engineering A*[J], 2018, 723(4): 30 359
19 Chen Zhen, Chen Shenggui, Wei Zhengying *et al*. *Progress in Natural Science: Materials International*[J], 2018, 28(4): 496
20 Zheng Guoming, Mao Xiaonan, Lei Li *et al*. *Vacuum*[J], 2019, 160: 81
21 Bahl S, Mishra S, Yazar K U *et al*. *Additive Manufacturing*[J], 2019, 28: 65
22 Casati R, Lemke J, Vedani M. *Journal of Materials Science and Technology*[J], 2016, 32: 738
23 Wang Youming, Li Manyun, Wei Guang. *Controlled Rolling of Steel and Controlled Cooling*[M]. Beijing: Metallurgical Industry Press, 2019: 8 (in Chinese)
24 Mao Weimin, Zhu Jingchun. *The Structure and Properties of Metallic Materials*[M]. Beijing: Tsinghua University Press, 2008: 200 (in Chinese)
25 Hu Jun. *Thesis for Doctorate*[D]. Shenyang: Northeastern University, 2014 (in Chinese)
26 Hanamura T, Yin F, Nagai K. *Transactions of the Iron & Steel Institute of Japan*[J], 2004, 44(3): 610
27 Xu Jinquan. *Theory on the Strength of Materials*[M]. Shanghai: Shanghai Jiaotong University Press, 2009: 70 (in Chinese)
28 Morris Jr J W. *Science*[J], 2008, 320(5879): 1022
29 Calcagnotto M, Adachi Y, Ponge D *et al*. *Acta Materialia*[J], 2011, 59(2): 658
30 Maria L M S, Miguel G Z, Kurt B *et al*. *Additive Manufacturing* [J], 2018, 23: 402
31 Yang Xiaolong, Xu Yunbo, Tan Xiaodong *et al*. *Materials Science and Engineering A*[J], 2014, 607: 53
32 Yang Xiaolong, Xu Yunbo, Tan Xiaodong *et al*. *Materials Science and Engineering A*[J], 2015, 641: 96

激光选区熔化 316L 奥氏体不锈钢微观组织和冲击韧性的各向异性

宗学文[1]，刘文杰[1]，杨雨蒙[2]，张树哲[3]， 陈 桢[3]

(1. 西安科技大学 机械学院，陕西 西安 710054)

(2. 中航光电科技股份有限公司，河南 洛阳 471023)

(3. 西安交通大学 机械工程学院，陕西 西安 710049)

摘 要：研究了激光选区熔化成形 316L 奥氏体不锈钢的微观组织和冲击韧性的各向异性，采用光学显微镜(OM)、X 射线衍射(XRD)、扫描电子显微镜(SEM)、电子背散射衍射(EBSD)对其微观结构进行表征，利用金属摆锤试验机进行冲击韧性试验。结果表明：激光选区熔化成形 316L 不锈钢的组织和冲击韧性存在着明显的各向异性，垂直和平行于 *Z* 向试样的物相均为 γ-Fe 相，垂直于 *Z* 向的组织呈“棋盘状”形貌，晶粒大多数为等轴晶形貌且晶粒得到了细化(d_{mean}=9.177 μm)，尤其熔池搭接区域晶粒更加细小(6 μm 以下)，而平行于 *Z* 向为“鱼鳞状”形貌，大多数为柱状晶形貌，晶粒直径较大(d_{mean}=21.247 μm)。同时垂直于 *Z* 向织构为强纤维织构<110>//RD 和弱板织构{112}<110>，而平行于 *Z* 向为强纤维织构<110>//RD。在致密度相同条件下，*X*/*Y*、*Z* 向的冲击韧性分别为 62.8±3.2 和 38.6±4.5 J，*X*/*Y* 向的冲击韧性明显优于纵向且提高了 62.69%。此外晶粒大小、大小角度晶界和织构类型对冲击韧性各向异性有着明显的影响，*X*/*Y* 向的晶粒得到了细化，大角度晶界数目多，韧性较好；纤维织构<110>//RD 对冲击韧性不利，而板织构{112}<110>有利于韧性，垂直 *Z* 向的<110>//RD 织构强度低且存在弱{112}<110>织构，韧性较好。

关键词：激光选区熔化；316L 不锈钢；微观组织；织构；冲击韧性；各向异性

作者简介：宗学文，男，1964 年生，博士，副教授，西安科技大学机械学院，陕西 西安 710054，电话：029-85583159，E-mail: zongw007@xust.edu.cn